JOURNAL OF APPLIED ELECTROCHEMISTRY 17 (1987) 983–996

Evaluation of electroactive intermediate states in anodic O_2 evolution at chemically formed nickel oxide: comparison with behaviour at nickel metal anodes

TONG-CHANG LIU*, B. E. CONWAY‡

Chemistry Department, University of Ottawa, 365 Nicholas Street, Ottawa, Ontario, Canada K1N 9B4

Received 30 June 1986; revised 2 January 1987

The behaviour of the kinetically involved intermediate states arising in the electrocatalysis of anodic oxygen evolution at chemically formed, high-area nickel oxide (NiO · OH) films on nickel metal as substrate is examined by means of analysis of potential (V) decay transients, following interruption of anodic polarization currents at various overpotentials. The potential decay behaviour is treated in terms of the dependence of $V(t)$ on log (time, t), and of ln $(-\mathrm{d}V/\mathrm{d}t)$ as f$[V(t)]$. The pseudocapacitance associated with the potential-dependence of the coverage or surface density of the overpotential-deposited species involved as intermediates in the reaction at the oxide electrode surface is evaluated jointly from the potential decay and Tafel polarization behaviour, following procedures developed recently.

In anodic O_2 evolution on oxide surfaces, such as NiO · OH, the intermediate states in the kinetics of the reaction are to be identified as OH or O species coupled with potential-dependent Ni(III) and Ni(IV) oxidation states of nickel, and the surface density of these states can be evaluated experimentally.

The results obtained for anodic O_2 evolution on the chemically formed nickel oxide films are compared with the behaviour at anodically formed thin oxide films on nickel metal.

1. Introduction

The electrochemical and adsorptive behaviour of electrocatalyst materials for the processes involved in water electrolysis is of current interest in electrochemical technology and in relation to fundamental aspects of the mechanisms of electrolytic H_2 and O_2 production [1, 2]. For optimization of polarization performance, it must be emphasized that a low Tafel slope, b $(=\mathrm{d}V/\mathrm{d}\log i)$, is as important as a favourable value of exchange current density (i_0), especially for electrolytic processes that are to be operated at moderately high current densities, i, as we have pointed out recently [3, 4]. In general, b is determined both by the symmetry factor, β, for electron exchange in a charge-transfer step *and* by the potential-dependence of coverage by intermediates that arise when the reaction is a multi-step surface process. However, it is surprising that, until recently [5–7], few experimental results have been available on the latter matter which is of major interest in electrode kinetics and especially electrocatalysis, as well as of being of concern in factors which can lead to practical diminution of power losses.

In recent papers [5–7] we have described results on evaluation of potential-dependence of coverage by the overpotential-deposited (OPD) species, H, that are the kinetically significant species in the cathodic H_2 reaction at appreciable faradaic currents. The methods of recording open-circuit potential decay [5, 8, 9], following interruption of polarizing current, and a.c.

* Visiting Scholar from the People's Republic of China.
‡ To whom correspondence should be directed.

0021–891X/87 $03.00 + .12

impedance [7, 11] were employed to derive information on the potential-dependence of coverage by H at cathodes of nickel, platinum, gold and electrodeposited nickel–molybdenum alloys. The results enabled the Tafel slope behaviour for cathodic H_2 evolution at these materials to be rationalized. The theoretical bases of these methods have been described previously [7, 12–16].

In the present paper the potential-decay method is applied to the examination of the potential-dependence of the surface density of intermediate states involved in the anodic oxygen evolution reaction (OER) at high area, chemically formed Ni(III) oxide material used as an electrocatalyst surface for the O_2 evolution reaction in aqueous alkaline solutions. We refer to the coverage of the electrode surface by intermediates in the reaction steps of anodic oxidation in terms of this 'surface density' rather than two-dimensional coverage by OH or O species because an oxide surface probably behaves, not like the surface of a metal lattice for H adsorption, in cathodic H_2 evolution for example, but actively participates in the O_2 evolution reaction sequence by changes of oxidation state of the metal ions coupled with changes of oxygen-to-metal ion stoichiometry that may arise in a surface region of small but significant thickness. This type of involvement of oxide surfaces in the anodic O_2 evolution reaction was proposed some time ago [17, 18] and has been taken up further by others [19–22].

Comparisons will be made with the electrode kinetic and adsorptive behaviour in the O_2 evolution reaction at compact, thin, nickel oxide films formed anodically on nickel metal.

The purpose of using the chemically formed, thick-film nickel oxide in this work was to be able to examine a material of possible practical significance, as electrode coatings of nickel oxide having a relatively high real-to-apparent area ratio, r, can be generated. Similar films of cobalt oxides can be formed.

For the present materials, r was found to be ~ 1000, as determined by *Kr* desorption BET measurements on a Quantasorb apparatus for real surface area determination. The real areas were determined on vacuum-dried, chemically formed oxide film electrodes, that had been previously washed free of NaOH. While these areas may not coincide exactly with the electrochemically significant areas, they provide a good basis for evaluation of the material as an oxygen evolution electrocatalyst.

2. Experimental details

2.1. *Methods*

Steady-state anodic polarization runs were performed at thick nickel oxide films, chemically formed on high-purity nickel wires by the procedure of Briggs *et al.* [23] using aqueous NaOCl. Polarization at each current density was performed for a controlled time at a potentiostatically fixed potential. The Tafel relations obtained by this procedure were very reproducible.

Potential relaxation transients, following interruption of the polarization currents at each of a series of potentials, were digitally recorded on two Nicolet digital oscilloscopes in tandem in order to cover six decades of time in the decay transients. The decay data, coupled with the steady-state polarization information, were processed in a PDP/11-34 computer to obtain the non-equilibrium pseudocapacitance of the electroactive states of the surface in the O_2 reaction, and other quantities as fully described in previous papers [5, 6]. Details will not be repeated here. The basis of interpretation of results obtainable from this experimental approach has also been given in earlier publications [9, 10, 12, 13, 17, 18]. The pseudocapacitance information gives the potential-dependence of the density in the surface region of the intermediate states involved in the O_2 evolution reaction at the nickel oxide surface.

Cyclic voltammetry experiments were conducted to provide a comparison of the Ni · O · OH oxidation–reduction behaviour in relation to the onset of anodic O_2 evolution. Several complementary experiments were performed to determine the a.c. impedance behaviour of the electrodes using a Solartron frequency response analyser.

2.2. *Preparation of electrode materials*

2.2.1. Chemically formed nickel oxide. High-purity nickel wires (Johnson Matthey and

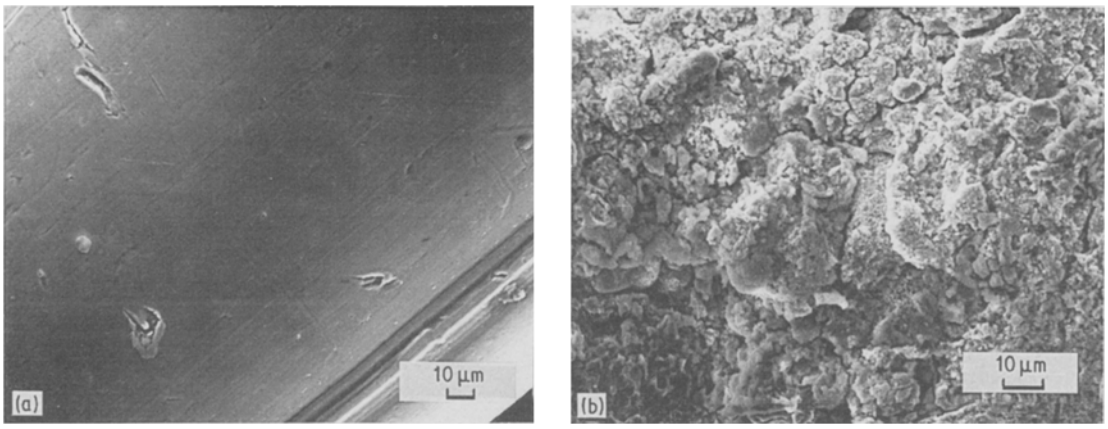

Fig. 1. Scanning electron micrographs of the surfaces of (a) anodically formed nickel oxide film, and (b) chemically generated oxide film.

Mallory, 99.99% Ni) were cleaned in acetone and then subjected to an oxidation treatment [23] in fresh aqueous NaOCl (active Cl_2, 12%) at 75° C for 3 min. This procedure produces a relatively thick, black oxide film, nominally of Ni · O · OH, on the nickel. The film material is electronically conducting and is similar to that in a charged nickel oxide battery plate. The scanning electron photomicrograph shown in Fig. 1a reveals a material of granular structure; the anodic film in Fig. 1b, by contrast, is almost smooth.

The chemically formed films were washed three times in doubly distilled water and then allowed to stand for 24 h in 0.1 M NaOH solution to ensure removal of Cl^- ions. No desorbable Cl^- remained after this treatment (acidic $AgNO_3$ test on the wash water). The electrodes were then used in a separate preparation of aqueous NaOH in a three-compartment polarization cell as in [5, 6].

2.2.2. Anodically formed films. The comparative measurements on anodically thin oxide films were conducted at nickel metal electrodes on which a nickel oxide film had been potentiostatically formed in 1 M aqueous NaOH for 1 h at a potential of + 0.6 V versus Hg/HgO. More detailed work on the anodically formed films will be presented in a forthcoming paper to be published elsewhere (*Faraday Trans. I* (1987)).

2.3. *Solutions*

Aqueous solutions of NaOH (0.2 M) were made up in doubly distilled water, the first stage being from alkaline permanganate. We have found that pyrodistilled water is not required for anodic work of this kind.

2.4. *Reference electrode*

A Hg/HgO electrode, made up in the same NaOH solution as that used for the polarization and potential relaxation measurements, was used as reference [cf. 17, 18]. This electrode was maintained in a separate cell compartment, semi-isolated from the working electrode compartment of the cell by means of a wetted, ungreased stopcock. Relative to the Hg/HgO electrode, the O_2 reversible potential in aqueous solution is 0.30 V at 298 K, independent of pH.

3. Treatment of polarization and decay data

The equations shown below, discussed previously [5, 6, 9, 10, 14, 15], are used to process the data and provide a basis [cf. 9, 10, 12, 13] for interpretation of the results. The significance and justification of these equations has been explained in previous papers [5–7, 9, 10, 12–15, 17, 18]. The electrode kinetic and derived quantities of interest are: (i) the pseudocapacitance, C_ϕ, of the intermediate states as a function of potential; (ii) the Tafel slopes of the polarization lines; (iii) the slopes of $V(t)$ versus log t or log $(t + \tau)$ (see below) relations characterizing the potential decay $[V(t)]$ behaviour; and (iv) the log $(-\mathrm{d}V/\mathrm{d}t)$ versus V behaviour.

The relevant equations are

$$-C\left(\frac{dV}{dt}\right) = i_0 \exp[\alpha VF/RT] \quad (1)$$

$$C = C_\phi + C_{dl} \quad (2)$$

and the Tafel relation, in exponential form, is

$$i = i_0 \exp \alpha VF/RT = i_0 \exp V/b_T \quad (3)$$

where i is the current density in A cm^{-2}, i_0 the corresponding exchange current density, α the transfer coefficient, V the overpotential, b_T is the Tafel slope of the logarithmic polarization line for the electrode process, C is the total interfacial capacitance made up of the double-layer capacitance, and C_ϕ is the pseudocapacitance associated with potential-dependence of coverage or surface density of states of adsorbed intermediates generated in the course of the anodic O_2 evolution reaction. C_ϕ is thus the pseudocapacitance associated with the 'overpotential-deposited' species arising at finite overpotentials of the overall reaction, as treated in terms of the kinetics of the reaction steps in the paper of Gileadi and Conway [24]. The kinetic approach to the solution of the course of potential decay on open circuit has been treated in [7, 9, 10, 12, 13].

For potential-independent values of C, Equation 1 integrates to

$$V(t) = -\frac{RT}{\alpha F} \ln (t + \tau) - \frac{RT}{\alpha F} \ln (i_0/b_T C) \quad (4)$$

where τ is an integration constant, $bC/i(t = 0)$. More generally, C is found as a function of V from analysis of the experimental potential decay curve by evaluation of $-dV/dt$ throughout the curve. This is the basis of the approach used in the present work as discussed in previous papers [5, 6, 14, 15, 17, 18].

The plot of $V(t)$ is linear in the log of the modified time variable, $t + \tau$, or of t itself when $t \gg \tau$. The slope of $-dV/d \ln (t + \tau)$ is equal to the Tafel slope, b_T, when C is constant or when C itself is limitingly an *exp* function of V; V is linear in $t + T$, but has a slope different from b_T. Usually when C is determined principally by C_ϕ, it is dependent on potential, cf. [17, 18, 24]. Also, it may be shown that the plot of $\ln (-dV/dt)$ versus V (which follows from Equation 1) has numerically the same slope as the $V(t)$ versus $\ln (t + \tau)$ relation for all conditions. Plots of $\ln (-dV/dt)$ versus V then avoid any arbitrariness in evaluating τ to obtain linear $V(t)$ versus $\ln (t + \tau)$ plots, and hence their slopes.

A theoretical evaluation of the potential decay method, based on an extension of [9, 10, 12, 13] through numerical solution of kinetic equations for various reaction steps that represent the processes involved in the decay behaviour, has been given recently [7]. It is found that Equation 1 represents the behaviour with $C \cong C_{dl}$ at short times of the decay profile, while C_ϕ principally determines the behaviour after longer times when a discharge followed by desorption reaction mechanism applies, with an electrosorbed intermediate, as in the H_2 or Cl_2 evolution reaction. Similar considerations apply to the O_2 evolution reaction except that more than a single intermediate may be involved.

4. Results and discussion

4.1. *Cyclic voltammetry*

In order to characterize the oxidation–reduction behaviour of the chemically formed nickel oxide films in comparison with the behaviour of anodically formed films on nickel metal, cyclic voltammograms were recorded, as shown in Fig. 2a, b. While the anodically formed oxide film shows the well-known cathodic and anodic peaks in the cyclic voltammograms (Fig. 2a), corresponding to the reduction of hydrated Ni · O · OH to $Ni(OH)_2$ and reoxidation of the latter to Ni · O · OH, the cyclic voltammogram (Fig. 2b) for the chemically formed film shows, principally, the current–potential relation for O_2 evolution on the anodic sweep and an unstructured profile on the cathodic sweep. These current profiles probably contain respective components due to O_2 evolution and reduction, superimposed on the active current components for partial oxidation or reduction of the oxide itself. Thus, in comparison with Fig. 2a it appears that significant O_2 evolution rates on the chemically formed oxide arise at *lower* potentials relative to those for the II to III and III to IV oxidation state changes of nickel in the oxide and at its surface. At nickel oxide battery plaque

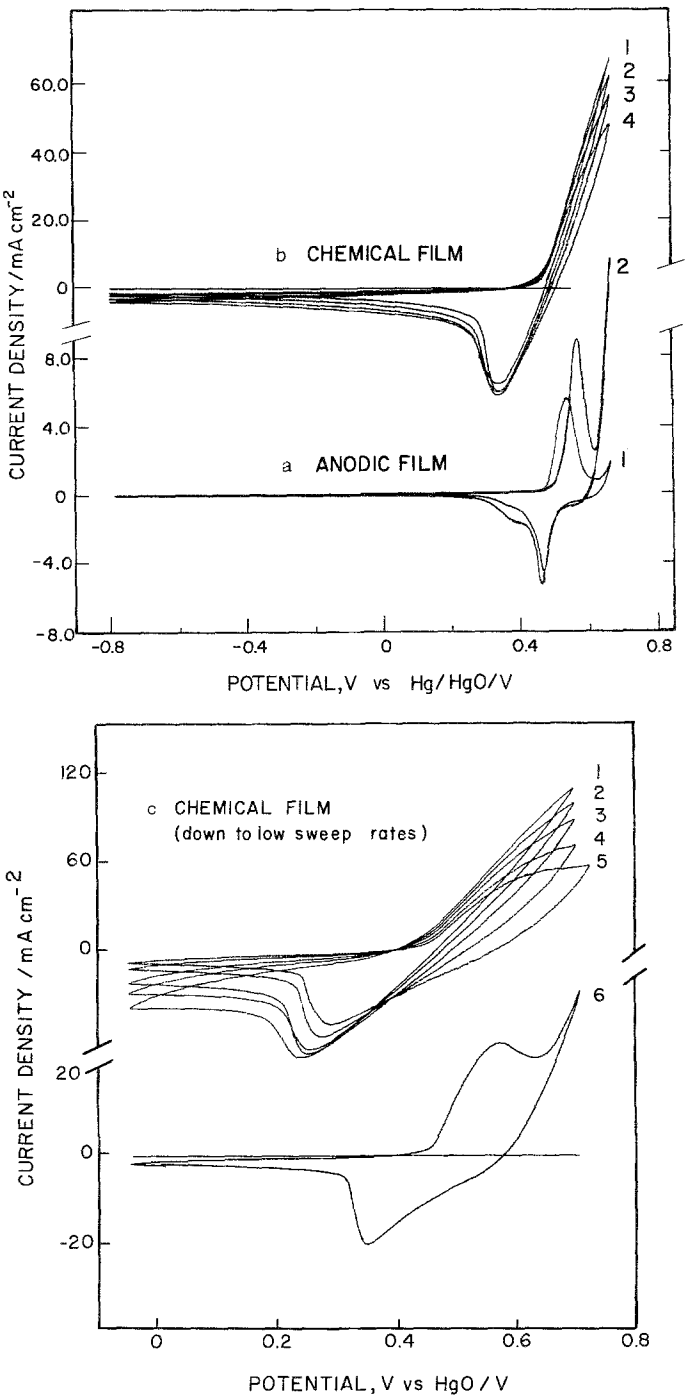

Fig. 2. Comparison of cyclic voltammograms for (a) anodically and (b) chemically formed nickel oxide films, including the region > 0.5 or 0.6 V (Hg/HgO) where O_2 evolution commences. (c) Chemically formed film down to a low sweep rate of 2 mV s^{-1}. (a) Direct anodic oxidation–reduction cyclic voltammogram at nickel at 200 mV s^{-1} (curve 1); after 1 h holding at 0.60 V (curve 2). (b) Voltammograms for chemically formed film at (1) 200, (2) 100, (3) 50 and (4) 20 mV s^{-1}. (c) For chemically formed film at 200 to 20 mV s^{-1} (curves 1 to 4 as in (b), respectively) and at 10 (curve 5) and 2 mV s^{-1} (curve 6). T = 298 K.

electrodes it is to be noted, cf. [28–30], that there is a rather continuous change of oxidation state from Ni(II) to Ni(IV) with increase of positive potential, and this is coupled [29] with increasing O_2 evolution rate both on anodic polarization and on open-circuit self-discharge [29]. The development of Ni(IV) oxidation states in the oxide and associated O_2 evolution depend appreciably on the concentration of the alkali supporting electrolyte and on temperature [17, 18].

It is interesting that only at very low sweep

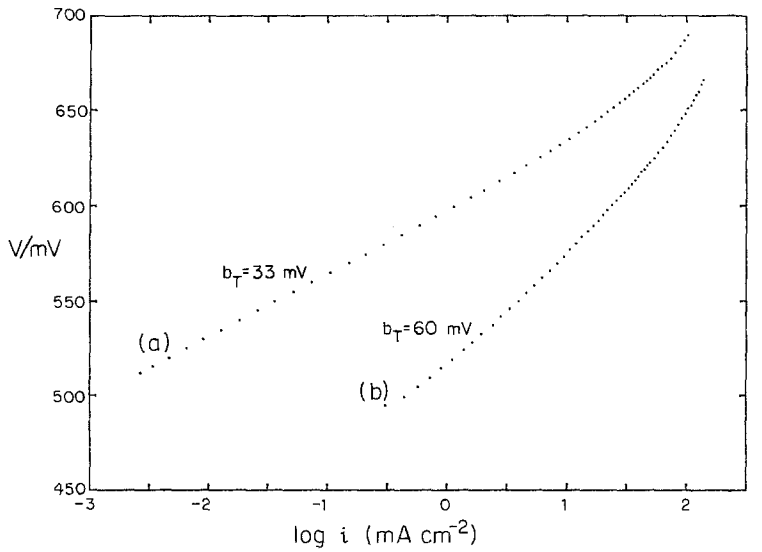

Fig. 3. Comparison of Tafel polarization behaviour for anodic O_2 evolution on (a) anodically and (b) chemically formed nickel oxide films at T = 298 K.

rates, below 2 mV s^{-1} (curve 6 of Fig. 2c) or 1 mV s^{-1} (not shown) do the anodic and cathodic peaks for change of oxidation state of the chemically formed oxide become resolved from the O_2 evolution and reduction faradaic current lines. At the chemically formed material, oxidation or reduction of the oxide evidently is much slower than at the anodic oxide film in the time scales of the sweeps employed, i.e. 5 s V^{-1} down to 500 s V^{-1}. This difference may be determined by the particle–particle contact in the thicker porous oxide film formed under the chemical conditions. Only under the slowest sweep conditions does the behaviour of the chemically formed material approach that of the anodically formed oxide shown in Fig. 2b, observed in that case at much higher sweep rates.

4.2. *Anodic polarization and open-circuit potential decay behaviour*

For analysis of the O_2 evolution behaviour and the pseudocapacitance associated with the kinetically involved species in the O_2 evolution reaction, using Equation 1, the Tafel polarization plots and the potential decay behaviour, following interruption of polarizing currents, are required.

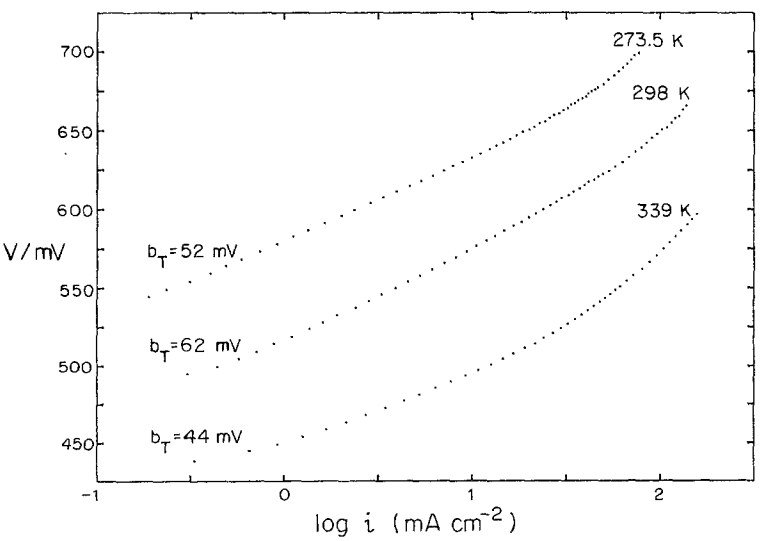

Fig. 4. Comparison of Tafel polarization behaviour for anodic O_2 evolution on chemically formed nickel oxide films at T = 273.5, 298 and 339 K.

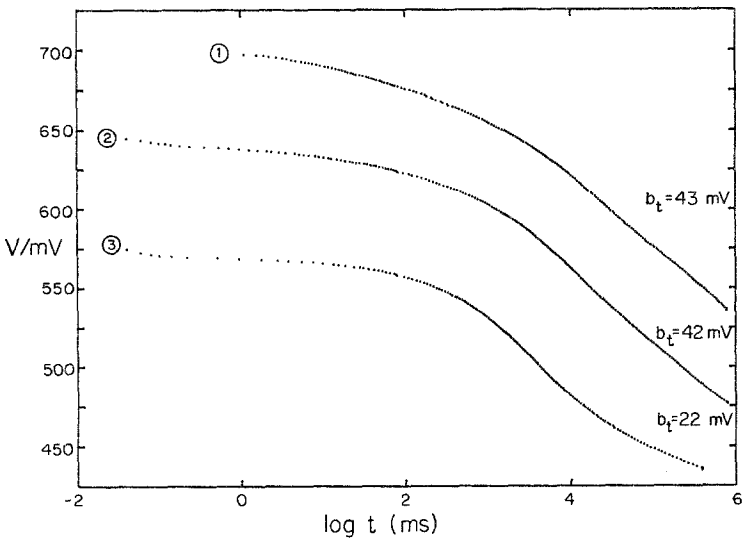

Fig. 5. Plots of $V(t)$ versus log t for open-circuit potential decay with the OER at chemically formed nickel oxide films at the following values of T (K): 1, 273.5; 2, 298; 3, 339 K.

Comparative anodic polarization plots for the chemically and anodically formed nickel oxide films are shown in Fig. 3. The anodically formed film (a) shows a lower Tafel slope (33 mV per decade) than that for the chemically formed film (b) (~ 60 mV per decade), but the activity in terms of attainable log i values is better for the chemically formed film, allowing for the real–apparent area ratio differences. Fig. 4 shows the Tafel relations for the chemically formed film at three temperatures. For V(Hg/HgO) = 0.550 V, these results correspond to an apparent activation energy of 31 ± 2 kJ mol^{-1}. All show an initially low slope region followed by a region of progressively higher slope. The data for the Tafel plots in Figs 3 and 4 are all 'iR' corrected from the initial potential drops observed on the Nicolet oscilloscope at the moment of current interruption in the potential decay experiments.

Evidently, from the Tafel behaviour, there is a specific mechanistic difference between the behaviour of the OER at chemically and anodically formed nickel oxide films that is not simply due to difference of real areas. This is already indicated in another way from the cyclic voltammograms of Fig. 2a, b.

The potential decay results are presented in two ways: as $V(t)$ versus log t and $V(t)$ versus log $(-\mathrm{d}V/\mathrm{d}t)$ plots. The former have different (negative) slopes from the Tafel relations for the same potential range if C in Equation 1 is potential-dependent [9, 10, 17, 18, 24] while $V(t)$ versus log t and log $(-\mathrm{d}V/\mathrm{d}t)$ should have the *same* numerical values of slope. It is to be noted that plotting $V(t)$ versus log $(-\mathrm{d}V/\mathrm{d}t)$ avoids the empirical procedure of evaluating the integration constant, τ, that arises in Equation 4 from integration of Equation 1.

Plots of these kinds are given in Figs 5 and 6 for T = 273.5, 298 and 339 K. Three regions are distinguishable in the log $(-\mathrm{d}V/\mathrm{d}t)$ plots: (i) a relatively flat region corresponding to short times and higher potentials, near the initial steady-state potential; (ii) a region of well-defined slope (42–43 mV for 273.5 and 298 K at intermediate potentials; and (iii) an asymptotic approach to the reversible potential at 298 and 339 K with initially a low slope of ~ 22 mV in that region. In the $V(t)$ versus log t plots of Fig. 5 the initial regions of the decay plots are dominated in the expected [8] way by the effect of τ (Equation 4) when $\tau > t$, giving a flat initial decay behaviour. Evidently, however, this flatness is not entirely due to the effect of τ, since Fig. 6 shows similar behaviour in log $(-\mathrm{d}V/\mathrm{d}t)$ at small t or high V. (Note, such behaviour is *not* observed [3–5] with the H_2 evolution reaction at short times, e.g. at nickel or gold.)

It is also useful to show how the $V(t)$ versus log t and log $(-\mathrm{d}V/\mathrm{d}t)$ plots depend on the prior steady-state current densities and corresponding overpotentials; such results are illustrated in Fig. 7a, b for steady-state current densities, prior to interruption, of 136, 106, 78, 42 and 25 mA cm^{-2}, all at 298 K. In these figures the expected agreement between $\mathrm{d}V(t)/\mathrm{d}$ log t and

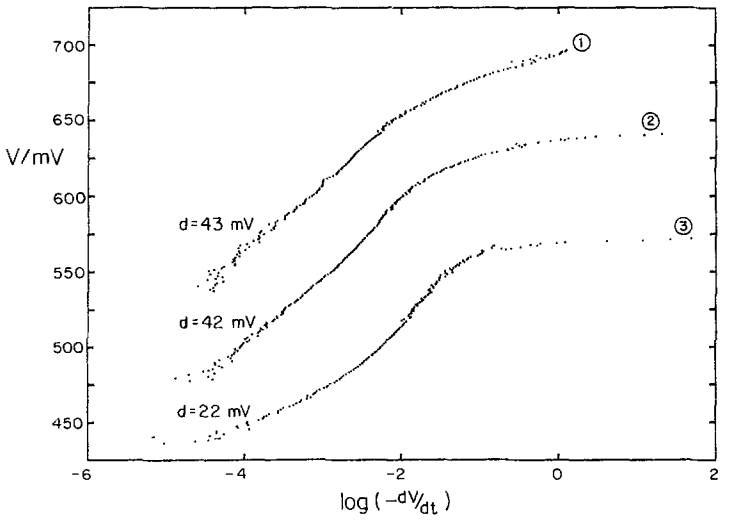

Fig. 6. Plot of $V(t)$ versus log $(-\mathrm{d}V/\mathrm{d}t)$ for conditions corresponding to those of Fig. 5.

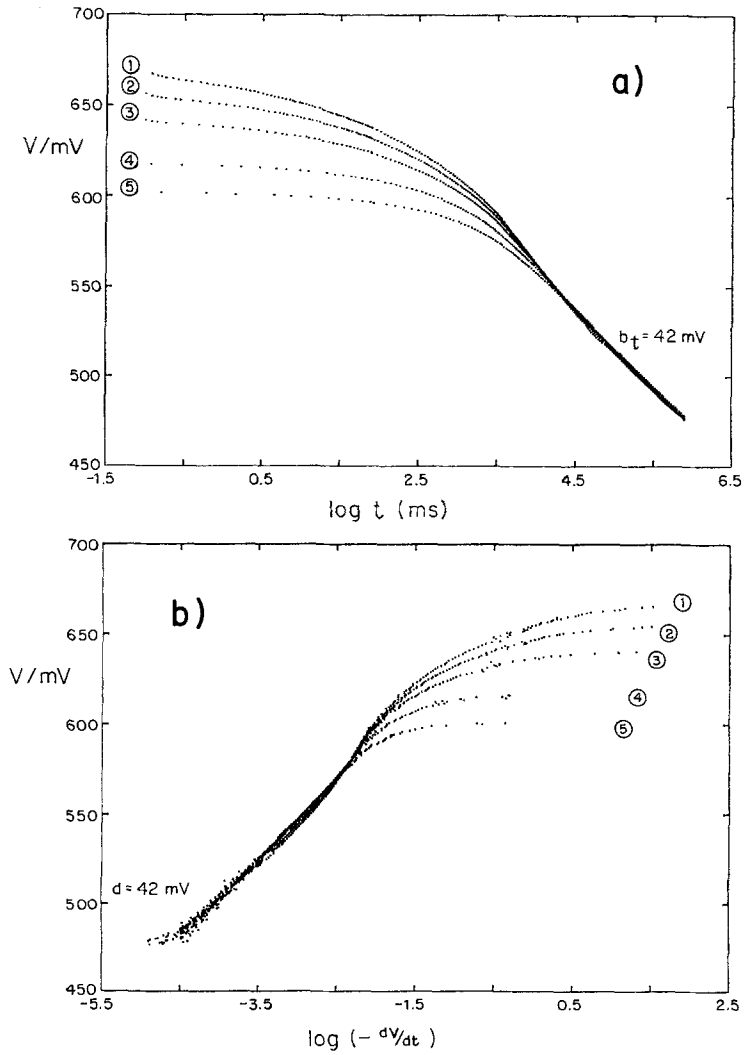

Fig. 7. (a) $V(t)$ plotted against log t for five initial current densities (mA cm^{-2}): 1, 136; 2, 106; 3, 78; 4, 42; 5, 25. $T = 298$ K. (b) $V(t)$ plotted against log $(-\mathrm{d}V/\mathrm{d}t)$ for the five initial current densities as in (a). $T = 298$ K.

Table 1. Comparison of potential-decay slopes, expressed as $dV(t)/d \log t$ *and* $dV(t)/d \log (-dV/dt)$, *with the Tafel slopes*[a] $dV/d \log i$ *for the OER at nickel oxide films at three temperatures*

T/K *(film)*	$dV/d \log i$ *(mV)*	$-dV(t)/d \log t$ *(mV)*	$dV(t)/d \log (-dV/dt)$ *(mV)*
273.5 (chemical)	52 (lower region) 75 (upper region)	43 ± 2	43 ± 2
298 (chemical)	52–62 (lower region) 75 (upper region)	42 ± 2	42 ± 2
339 (chemical)	48–52 (lower region) 80 (upper region)	24 ± 4 (lower region) 42 ± 4 (upper region)	24 ± 4 (lower region) 42 ± 4 (upper region)
298 (anodic)	37 (lower region) ≧65 (upper region)	28 (lower region) 58 (upper region)	28 (lower region) 58 (upper region)

[a] Tafel plots based on 55 to 60 points over 3.5 decades of i.

$dV(t)/d \log (-dV/dt)$ is seen for the linear regions below ~ 570 mV. The relations between the slopes of these plots (for regions that are reasonably linear) and the Tafel slopes for the same ranges of potential are recorded in Table 1.

It is seen from Figs 3 and 4 in relation to Figs 5 and 6, and from the data in Table 1, that the slopes $-dV(t)/d \ln t$ or $dV(t)/d \ln (-dV/dt)$ differ significantly from the Tafel slopes $dV/d \ln i$. As mentioned above and as follows from [9, 10, 13, 14, 17, 18] this implies that the capacitance C (Equation 1) is potential-dependent over the range of decaying V. Such behaviour is confirmed from direct evaluation of $C(V)$ from Equation 1 using the experimentally evaluated derivative $(-dV/dt)$ over the range of $V(t)$ as described in the section which follows.

4.3. *Adsorption pseudocapacitance of the intermediates and potential-dependence of their coverage or surface density*

From Equation 1, C can be derived as a function of potential over the range of potentials covered in the transient. Fig. 8 shows the $C(V)$ versus V behaviour at $T = 273.5$, 298 and 339 K for the OER at the chemically formed nickel oxide electrode. The curves for the three temperatures are essentially similar in shape with (i) an initially descending region, (ii) a plateau at 2300 to 3100 mF cm^{-2}, and (iii) a descent to small values towards the double-layer capacitance. (Note, this region corresponds to the initial 'flat' regions of the curves of $V(t)$ versus log t or $V(t)$ versus log $(-dV/dt)$, Fig. 7a, b.) These data, taken in separate experiments at three different temperatures, serve to exemplify the reproducibility and resolution of the potential decay method employing digital data acquisition and computer processing of the acquired data.

It is seen that the shift of the $C(V)$ versus V profile with temperature corresponds to a shift of potential, at which a given C is attained, by 1.4 mV K^{-1}. This would correspond to a very large apparent entropy change if the process involved were reversible; however, this temperature coefficient more probably reflects a *kinetic* effect in C since C_ϕ corresponds to a *non*-equilibrium pseudocapacitance [24] associated with the state of intermediates generated at appreciable currents.

Numerical simulations of the capacitance behaviour derived from potential decay transients suggest [7] that the lowest C values reached at the highest potentials correspond to double-layer capacitance C_{dl} while in the plateau region, C corresponds to $C_{dl} + C_\phi$, the pseudocapacitance of adsorbed intermediates. It seems that maxima tend to be reached in the profiles of Fig. 8 but are obscured by the further ascending $C(V)$ region. Reference to the cyclic voltammetry profiles in Fig. 2 suggests that this second, rising region is associated with pseudocapacitance arising from the potential-dependence of the state of oxidation of the bulk nickel oxide near its surface. The surface states of oxidation, Ni^{3+} and Ni^{4+}, are closely connected with the adsorbed intermediates, OH and O, in the OER, and 'diffusion' of the state of oxidation of the surface by H^+ and e transfer constitutes a mech-

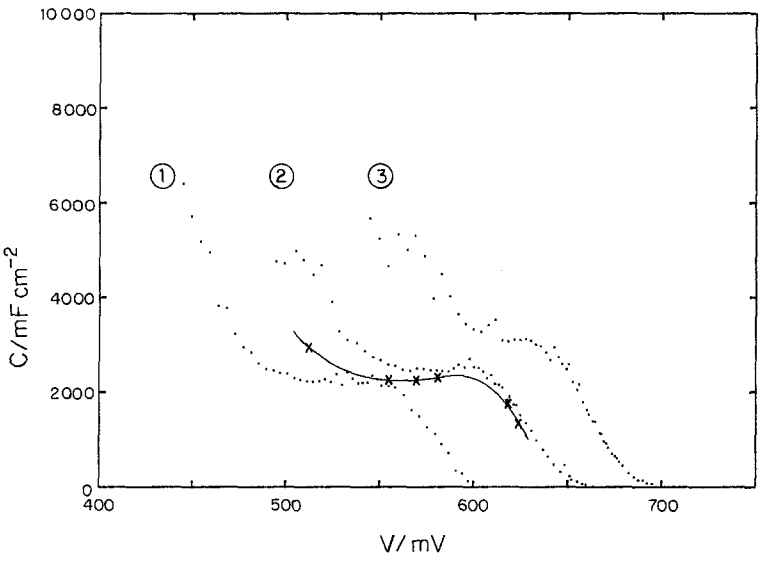

Fig. 8. Pseudocapacitance versus potential profiles for OPD intermediate species in the OER at nickel oxide electrodes at T values of 1, 339; 2, 298; 3, 273.5 K, derived from the potential-decay transients. Points marked × are from a.c. capacitance at 298 K.

anism for charging of the bulk nickel oxide, or its discharge on open-circuit [29].

Integration of the $C(V)$ profiles with respect to V gives the change of charge, Δq, involved in causing a change of state of the surface in the OER as potential is changed on open circuit. Fig. 9 shows plots of Δq, derived as $C\mathrm{d}V$, as a function of anode potential over the region of active O_2 evolution. Corresponding to Fig. 8, these curves are displaced to more positive potentials with decrease of temperature reflecting, as known with battery oxide material, a greater stability of more highly oxidized states of the material at lower temperatures. The effect is evidently quite large and also corresponds to the activation energy and related temperature dependence of the kinetics of the OER (Fig. 4). Attainment of a given oxidation state of the electrode or charge for development of surface density of intermediates requires higher potentials at lower temperatures.

It was noted earlier that the potential decay profiles were somewhat dependent on the initial current density for O_2 evolution (and corresponding η). Fig. 10 shows the series of $C(V)$ versus V profiles that result at 298 K from those transients. The same shapes of the profiles are observed, but decay from higher current densities tends to give a more extended $C(V)$ profile with a better defined maximum. This is probably

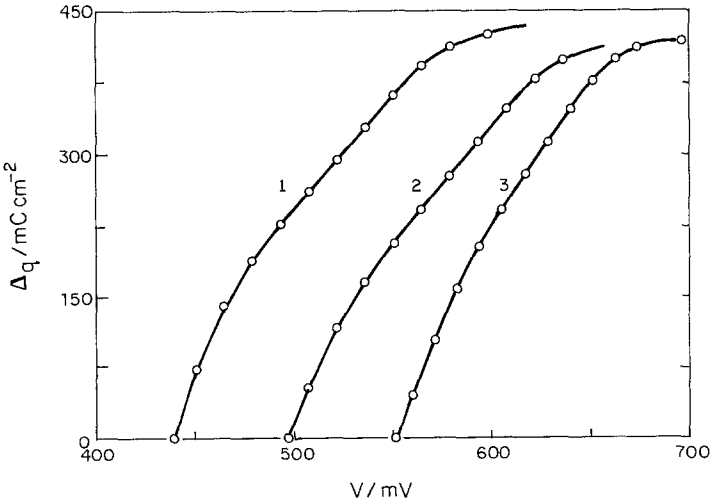

Fig. 9. Changes of charge, Δq, for change of surface density of intermediates in the OER at nickel oxide electrodes derived from Fig. 8 for the three temperatures (K): 1, 339; 2, 298; 3, 273.5.

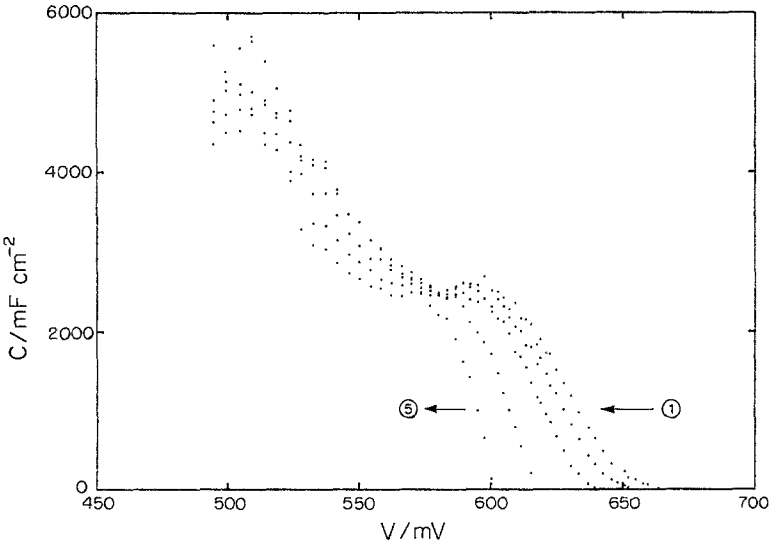

Fig. 10. Pseudocapacitance versus potential profiles for the OPD species, as in Fig. 8, following interruption of currents of 136, 108, 78, 42 and 25 mA cm^{-2}. Data for 298 K, from Fig. 7a.

because, at higher i, a higher state of local surface oxidation is attained. In contrast, the capacitance in the potential region we associate with changes of bulk state of oxidation is smaller, so that the maximum in C is better distinguished (Fig. 10).

The magnitude of the capacitance in the region of the maximum is ~ 2500 mF cm^{-2}. The BET real area determination gives a real apparent area factor of $\sim \times 1000$. Hence the C is about 2500 μF per real cm^2. This is in quite good agreement with that expected for development of a monolayer of electrosorbed O species, without appreciable interaction, requiring one electron per particle chemisorbed, and also agrees well with the capacitance maximum observed at anodically formed nickel oxide films that have much smaller real apparent area ratio. Correspondingly, the limit of q attained at the highest overpotentials is ~ 440 mC cm^{-2} or ~ 440 μC per real cm^{-2} (Fig. 9).

4.4. *Comparison of behaviour of chemically and anodically formed nickel oxide electrodes for the OER*

The difference of cyclic voltammograms (Fig. 2) and Tafel polarization behaviour (Fig. 3) has already been referred to earlier.

Figs 11 and 12 show comparisons of the $V(t)$

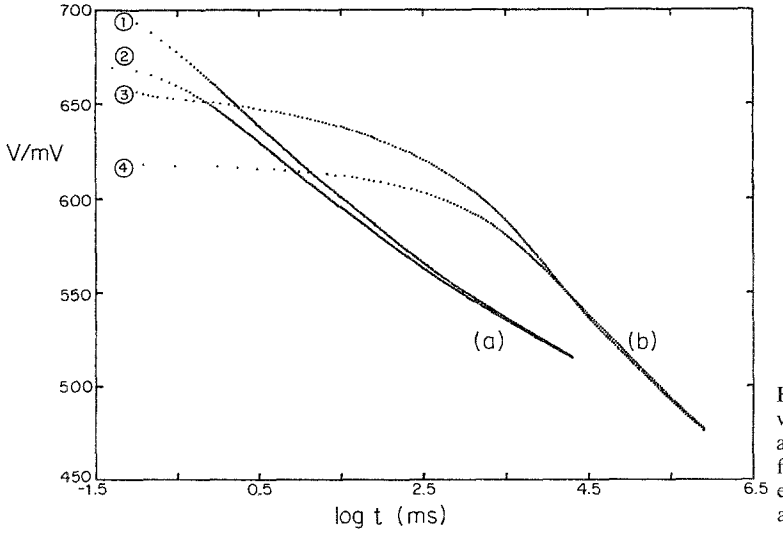

Fig. 11. Comparison between $V(t)$ versus log t points at 299 K for the OER at (a) anodically formed nickel oxide film and (b) chemically formed film, each for decay from two initial currents and corresponding potentials.

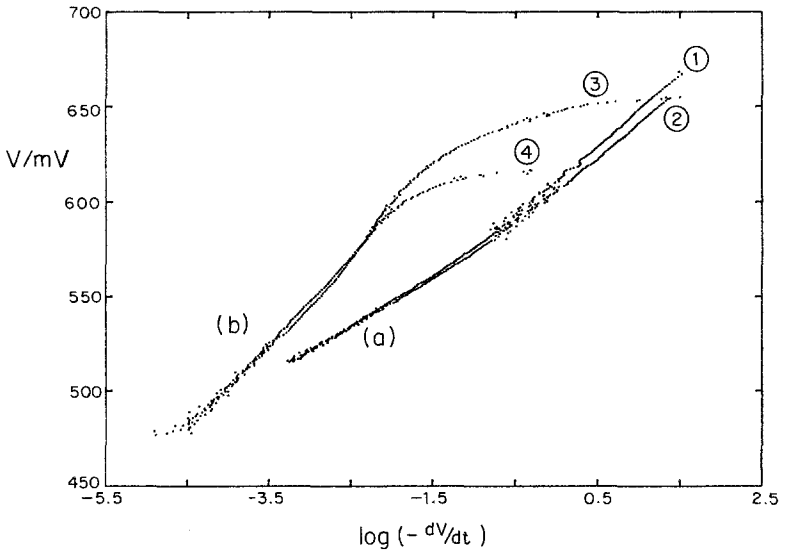

Fig. 12. Comparison between $V(t)$ versus log $(-\mathrm{d}V/\mathrm{d}t)$ plots at 299 K, as in Fig. 11, at (a) anodically formed film and (b) chemically formed film. Numbers on curves correspond to those on Fig. 11.

versus log t and $V(t)$ versus log $(-\mathrm{d}V/\mathrm{d}t)$ plots for potential decay in the OER at chemically and anodically formed nickel oxide films at 299 K. Two principal differences are observed. (i) The chemically formed material that has high specific area and is no doubt porous (Fig. 1), shows the long delayed decay of potential (Fig. 11) and a corresponding 'flat' region in Fig. 12 at high potentials. This behaviour is not seen in the corresponding plots for the anodically formed oxide films. (ii) In the linear regions of the plots, the slopes are $\mathrm{d}V/\mathrm{d}\log t = -43$ mV and -24 mV per decade, and $\mathrm{d}V/\mathrm{d}\log(-\mathrm{d}V/\mathrm{d}t) =$ 42 mV and 24 mV, respectively, for the chemically and anodically formed oxide films (Table 1).

Fig. 13 shows the comparison of the pseudocapacitance profiles as a function of potential for the OER at the two types of films. Again, a clear difference is manifested. The range of change of C is much greater for the chemically formed film and C rather rapidly approaches the limiting small double-layer capacitance between $E_{\mathrm{Hg/HgO}} = 650$ and 700 mV while the effect is less at the anodically formed oxide film. The plateau region is seen in both cases between potentials of ~ 0.580 and 650 mV. The data compared here

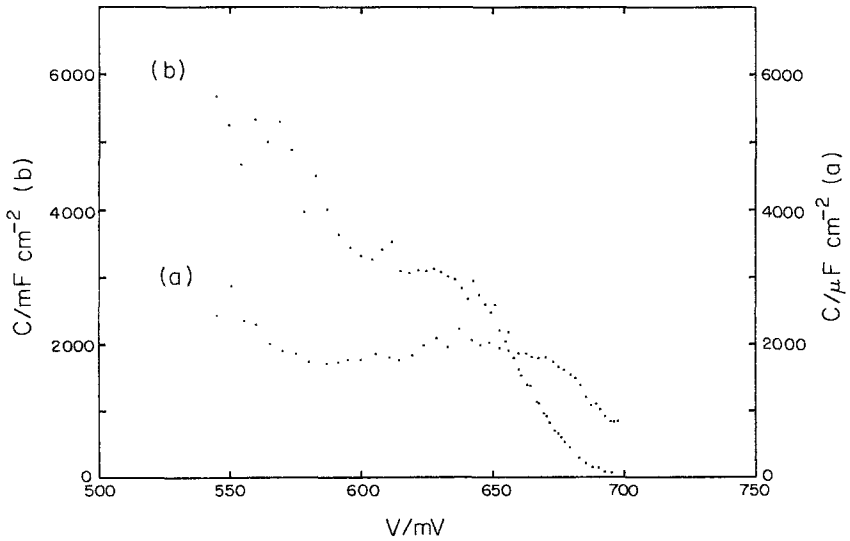

Fig. 13. Comparison between the pseudocapacitance versus potential profiles for the OPD species in the OER at (a) anodically formed and (b) chemically formed nickel oxide films at 273.5 K.

are for 273.5 K. The comparative behaviour at 299 K is qualitatively similar. After allowance for differences of real surface area, it is clear that there are substantial differences of the adsorption behaviour of the two types of nickel oxide material with respect to the intermediates in the OER, as well as of the kinetics of the process at the two types of surfaces.

4.5. *Comparison with a theoretical transient*

Computer simulation of potential decay transients that arise for a discharge step, producing an electrosorbed intermediate, followed by either an electrochemical desorption step or a chemical catalytic recombinative desorption was recently carried out by Harrington *et al.* [7] in this laboratory. Four regions of the transient were identifiable (Fig. 14). (i) An initial region where the self-discharge is mainly that of the double-layer capacitance and the pseudocapacitance is close to the steady-state value when the polarizing current was previously passing. This region corresponds to $t \ll \tau$. (ii) A region of linear decay of V in log t. (iii) A plateau region, depending on the mechanism. (iv) A final decay towards the reversible potential of the process. In the experimental transients for the OER, regions (i), (ii) and (iv) can be distinguished (see Figs 5 and 7), depending on initial conditions.

The mechanisms of the OER differ significantly from that considered by Harrington *et al.* and for H_2 or Cl_2 evolution in that the process is a four-electron one so there must be an extra step in the mechanism [21, 23], e.g.

$$OH^- + MO \rightleftharpoons MO \cdot OH + e \qquad \text{I}$$

$$MO \cdot OH \longrightarrow MO \cdot O + H^+ + e \qquad \text{II}$$

$$2MO \cdot O \longrightarrow MO + O_2 \qquad \text{III}$$

or

$$MO \cdot O + OH^- \longrightarrow MO + O_2 + H^+ + 2e \qquad \text{IV}$$

As with the H_2 reaction, O_2 can be generated either entirely by successive electrochemical pathways (I, II and IV) or by a pathway involving both electrochemical and chemical steps, i.e. I, II and III. In the above, 'MO' represents an initial state of the oxide surface.

The Tafel slope behaviour of the OER at nickel oxide surfaces does not indicate the recombination step III as rate controlling (III gives a slope $RT/4F$ under Langmuir conditions, which is not observed).

5. Summary and conclusions

By means of digital recording of potential decay transients following interruption of anodic polarization of chemically and anodically formed nickel oxide electrode surfaces, the behaviour of the kinetically involved intermediates in the anodic O_2 evolution reaction is obtained. The potential decay behaviour, $V(t)$, is represented by means of plots as functions of log t and

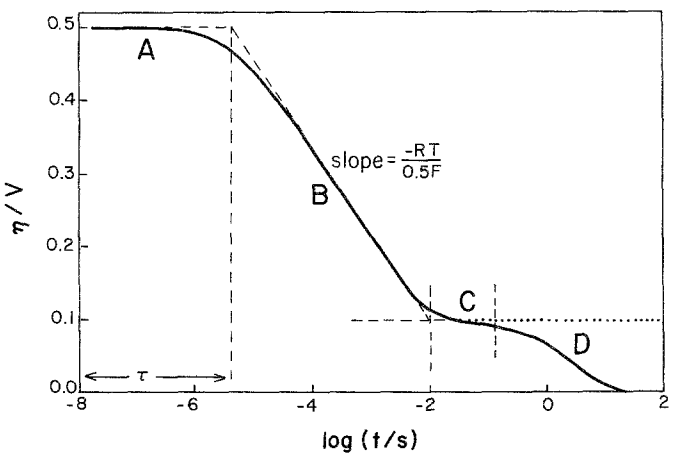

Fig. 14. Theoretical potential-decay transient for an electrochemical desorption controlled process, following discharge of an electrosorbed intermediate, calculated by computer simulation. (From Harrington *et al.* [7], based on solution of non-steady state equations $(q_1/F)(d\theta/dt) = v_1 - v_2$ and $-(C_{dl}/F)(d\eta/dt) = v_1 + v_2$, where v_1 and v_2 are the velocities of the discharge and desorption steps, respectively, q_1 is the monolayer charge for deposition of the intermediate and C_{dl} is the double-layer capacitance.) Four distinguishable regions, A, B, C and D, are indicated in the time course of the transient. Calculations are for rate constants $k_1 = 10^{-9}$, $k_{-1} = 10^{-8}$, $k_2 = 10^{-10}$ and $k_{-2} = 10^{-11}$ mol cm^{-2} s^{-1}, $q_1 = 210\,\mu$C cm^{-2}, $C_{dl} = 25\,\mu$F cm^{-2} and initial overpotential η (see [7]) is taken as 0.5 V. For significance of k values see [7].

ln $(-dV/dt)$, the slopes of which are to be compared with those of the Tafel relations determined under the same conditions.

Computer processing of the acquired potential relaxation data enables the pseudocapacitance associated with the potential-dependence of the surface density of the OPD intermediate states to be evaluated quantitatively over a range of potentials.

The behaviour of the chemically formed nickel III oxide surface is found to be appreciably different from that of compact, anodically formed films in the following respects: (i) the Tafel polarization slopes are different; (ii) the profiles of $V(t)$ versus log t or log $(-dV/dt)$ are different and the form of $C(V)$ versus V is different.

Values of $C(V)$ are also much larger for the chemically formed films than for the anodically formed film, as expected from the different real–apparent area ratios. Evidently, however, the electrochemical behaviour of the chemically formed film does not differ from that of the anodically formed film just on account of the larger area of the former material. Probably the chemically prepared oxide has a greater proportion of Ni(III) and Ni(IV) present as surface states on this high-area material, and this leads to the observed difference of the kinetic behaviour of the OER at the two types of nickel oxide films. This difference is already qualitatively manifested in the different shapes of the cyclic voltammograms (Fig. 2).

Acknowledgement

Grateful acknowledgement is made to the Natural Sciences and Engineering Research Council of Canada for support of this work.

References

[1] D. E. Frown, M. N. Mahmood, A. K. Turner, S. M. Hall and P. D. Rogarty, *Int. J. Hydrogen Energy* **7** (1982) 405.
[2] M. H. Miles, G. Kissel, P. W. T. Lu and S. Srinivasan, *J. Electrochem. Soc.* **123** (1976) 332; see also 'Comprehensive Treatise on Electrochemistry', Vol. 2, various chapters, (edited by E. Yeager, J. O'M. Bockris and B. E. Conway), Plenum Publ. Corp., New York (1981).
[3] B. E. Conway, H. A. Kozlowska, B. V. Tilak and M. A. Sattar, *J. Electrochem. Soc.* **130** (1983) 1825.
[4] Proc. VIth World Hydrogen Energy Conference, Vienna (1986), Pergamon Press (1987).
[5] B. E. Conway and L. Bai, *J. Chem. Soc., Faraday Trans. I* **81** (1985) 1841.
[6] *Idem,* in Proc. Vth World Hydrogen Energy Conference, Toronto, Canada (1984), Marcel Dekker, New York (1985) p. 879.
[7] D. A. Harrington, L. Bai and B. E. Conway, *J. Electroanal. Chem.* **221** (1987) 1.
[8] H. B. Morley and F. E. W. Wetmore, *Can. J. Chem.* **34** (1956) 359.
[9] B. V. Tilak and B. E. Conway, *Electrochim. Acta* **21** (1976) 745.
[10] *Idem, ibid.* **22** (1977) 1167.
[11] R. D. Armstrong and M. Henderson, *J. Electroanal. Chem.* **39** (1972) 81.
[12] B. V. Tilak, C. Rader and B. E. Conway, *Electrochim. Acta* **21** (1976) 745.
[13] *Idem, ibid.* **22** (1977) 1167.
[14] A. G. C. Kobussen and C. Mesters, *J. Electroanal. Chem.* **115** (1980) 131.
[15] A. G. C. Kobussen, H. Willems and G. H. Broers, *ibid.* **142** (1982) 67, 85.
[16] J. F. Armstrong and J. A. V. Butler, *Trans. Faraday Soc.* **29** (1933) 1261.
[17] B. E. Conway and P. L. Bourgault, *Can. J. Chem.* **38** (1960) 1557.
[18] *Idem, ibid.* **40** (1962) 1690.
[19] S. Trasatti, *J. Electroanal. Chem.* **111** (1980) 125.
[20] H. Tamura, *Denki Kagaku* **48** (1980) 173.
[21] A. Tseung, *Electrochim. Acta* **22** (1977) 31.
[22] P. Rasiyah and A. C. C. Tseung, *J. Electrochem. Soc.* **131** (1984) 803.
[23] G. W. D. Briggs, E. Jones and W. F. K. Wynne-Jones, *Trans. Faraday Soc.*, **51** (1955) 1433.
[24] E. Gileadi and B. E. Conway, *J. Chem. Phys.* **39** (1963) 3420.
[25] J. Weininger and M. W. Breiter, *J. Electrochem. Soc.* **110** (1963) 484.
[26] *Idem, ibid.* **111** (1964) 707.
[27] M. A. Sattar and B. E. Conway, Performance Forecast of Selected Static Energy Conversion Devices, 29th Meeting of ARGARD Propulsion and Energetics Panel, Liège, Belgium, June, 1967, Conference Proc. (edited by G. W. Sherman and L. Devon), US Air Force Aero Propulsion Lab., Dept. of the Air Force, Washington, DC, pp. 79–124.
[28] B. E. Conway and E. Gileadi, *Can. J. Chem.* **40** (1962) 1933.
[29] B. E. Conway and P. L. Bourgault, *ibid.* **37** (1959) 292.
[30] F. Kornfeil, Proc. Ann. Battery Research and Development Conference, 12th Conference US Army Signal Corps. (1958).
[31] J. O'M. Bockris, *J. Chem. Phys.* **24** (1956) 817.